Title: Electronic and Transport Properties of Sr doped Mg2Si Thermoelectric Material

Getu Tilahun Melesse[1], Mulualem Abebe Mekonnen[1]

[1]Faculty of Materials Science and Engineering, Jimma Institute of Technology, JImma, 378, Ethiopia.

Abstract

We investigated the electronic structure, dynamic stability, optical, and thermoelectric properties of strontium doped Mg_{2-x} $SiSr_x$, x = 0, 1, using First Principle approach with ultra-soft pseudopotential method to treat the interaction between the valence electron and the ion core and the Generalized Gradient Approximation (GGA) in Perdex Burke Emzerhof (PBE) form is used to process the exchange-related energy function. Sr modified Mg_2Si show good agreement with the experimental result for the electronic and thermoelectric properties. With semiclassical Boltzmann transport theory, the transport properties of Mg2Si and Sr doped Mg2Si alloys have been investigated systematically. The result of DFT conformed that, the undoped Mg_2Si system has indirect energy gap to a value of 0.222 eV; Sr doped 2x1x1 Mg_2Si supercell, showing direct bandgap with a value of 0.195 eV. The carrier concentration of Sr doped Mg_2Si thermoelectric material increased. After the doping, the fermi level shifts towards the conduction band and comprises of via a strong hybridization between the Sr-s, Si-p, Mg-s, and Mg-p orbitals, indicating that the covalent bonds formed by Sr, Si, and Mg atoms is very strong. The electrical conductivity of Sr doped Mg_2Si material is due to electrons, which is justified from the negative value of the Seebeck coefficient and its value increases with temperature. The lattice thermal conductivity dominates the electronic thermal conductivity as a function of temperature for Sr doped Mg2Si system.

In this work, the Sr-doped Mg_2Si materials were found to be a better thermoelectric material with increased Seebeck coefficient, electrical conductivity, and corresponding electronic thermal conductivity at a high-temperature range.

Keywords: Thermoelectric, Seebeck Coefficient, Optical property, Thermal Conductivity.

1. Introduction

Mg_2Si is a promising semiconductor material and related alloys are important for thermoelectric applications because of their environmental friendliness, low cost, abundance, and lack of toxicity, thermal stability, and low density. Silicides are very important materials with a wide range of technological applications. Recently, semiconducting silicides (Mg_2Si) attract researchers' attention due to their potential applications in thermoelectric, optoelectronics and photovoltaics [1-3]. To recover energies from thermal energies which are supposed to be wasted, thermoelectric devices are used to convert thermal energy to useful electrical energy. Mg_2Si is an excellent material for thermoelectric power generation due to its high Seebeck coefficient, high electrical conductivity and low thermal conductivity [4-6].

The two well-known approach to enhance zT are: (i) reducing lattice thermal conductivity(k_L) due to phonon scattering [7-9], (ii) improving the power factor ($S^2\sigma$) through the electrical transport properties [10, 11].

Jinfeng et al. reported the lattice thermal conductivity of BaMgSi is 1.27 W/mK at 300 K by using combination of first-principles density functional theory calculations and Boltzmann transport theory [12]. Solid solution of $Mg2Si_{1-x}Sn_x$ show ZT_{max} = 1.1 in the temperature range 600-870 K which put them among the best n-type thermoelectric materials, reported by V. K. Zaitsev et al.,[13]. H.L. Liu et al. [14] and L.D. Zhao et al. [15] have reported single crystals SnSe show low value of lattice thermal conductivity, $k_L = 0.23 \pm 0.03\ Wm^{-1}K^{-1}$ and an enhanced zT of 2.6 ± 0.03 at 923 K due to anharmonicity of lattice. Point defects [16, 17], dislocations [18, 19], grain boundaries [20 - 22], are supposed to be sources of phonon scattering which in turn reduces the lattice thermal conductivity (k_L) due to shorten phonon relaxation time.

The constituent elements for Mg2Si material are abundant, cheap, light weight and nontoxic. Moreover, Mg2Si is an attractive material with a novel applications in silicon based optoelectronics, integrated circuits and energy harvesting microsystems since silicide technology exhibits a unique compatibility with today's silicon-based microelectronics.

The crystal structure of Mg_2Si crystallizes is face centered cubic (fcc) phase with space group symmetry$Fm\bar{3}m$, at room temperature and atmospheric pressure.

To our best knowledge, no detailed first-principles density functional theory calculation combined with Boltzmann transport property data available for $Mg_{2-x}Sr_xSi$ (x = 0, 0.1) systems. In this article, we present a comprehensive ab-initio density functional (DFT) and Boltzmann transport theory study of the electronic structure, elastic constants, the optical and transport properties of $Mg_{2-x}Sr_xSi$ (x = 0, 0.1) systems.

2. Computational Methodology

We used a 2x1x1 Mg_2Si supercell and replacing the Mg-site with strontium (Sr) atom which act as an electron donor at Mg-site. Mg_2Si is an antifluorite face-centered cubic (FCC) structure with space group of Fm-3m, number 225 is illustrated in Figure 2. The optimized lattice constant was determined through calculations for the primitive is 6.3562 Å which is 0.62 % overestimated to the experimental value 6.35 Å [23].

Density Functional Theory (DFT) of first-principles calculations are used to perform all calculations using the Cambridge Serial Total Energy Package in Material Modeling, Accelrys (CASTEP) code [24, 25]. The interaction between the valence electron and the ion **core is** treated with ultra-soft pseudopotential. The valence electrons of Mg and Si atoms are treated as: Mg $2p^6$ $3s^2$ and Si $3s^2$ $3p^2$. The Generalized Gradient Approximation (GGA) in Perdex Burke Emzerhof (PBE) form [26] is used to process the exchange-related energy function with a cut-off energy of 300 eV. In the total-energy calculations, integrations over the Brillouin zone were performed using a 6x6x6 Monkhorst–Pack set [27]**.** The electron–ion interaction is described using Vanderbilt's ultrasoft pseudopotentials [28].

Self-consistency is achieved by setting the thresholds to 10^{-7} eV/cell for the total energy convergence as a criteria. The force convergence criterion is used as the average force acting on each atom less than 0.02 eV/Å. Subsequently, a very thin k-point mesh (20 × 20 × 20) has been used to obtain a precise description of the band structure of the slab models for use in the transport calculations.

In the second step the Boltzmann transport equation has been solved using the constant relaxation time approximation to determine the thermoelectric coefficients, namely, the Seebeck coefficient and the electrical conductivity, from the calculated electronic band structures as described above. The BoltzTraP program [29] has been used.

3. Results and Discussion

3.1 Crystal structures and bonding characteristics

In Mg_2Si compound Mg and Si atoms are located at Wyckoff positions 8c (0.25, 0.25, 0.25) and 4a (0, 0, 0), respectively. Energy-lattice parameter behaviors of the cubic crystalline phases of
In Mg2Si compound Mg and Si atoms are located at Wyckoff positions 8c (0.25, 0.25, 0.25) and 4a (0, 0, 0), respectively. Energy-lattice parameter behaviors of the cubic crystalline phases of Mg2Si with a space group of Fm-3m is shown in Figure 1. The optimized lattice parameter for this structure is 6.3562Å, which is slightly overestimated by 0.62 % as compared to experimental result [23]. The magnesium atom is coordinated with four silicon atoms with a bond length of 2.752 Å.

Bond energy may be a measure of a chemical bond‘s strength, meaning that it tells us how likely a pair of atoms is to stay bonded within the presence of energy perturbations. Alternatively, it are often thought of as a measure of the steadiness gained when two atoms bond to every other, as against their free or unbound states. In general, the stronger the bond between two atoms, the lower the energy minimum is and therefore the smaller the bond length.

Abebe et al. [30] shows that a higher degree of covalent would manifest as decrease in the Ti-O distance. We found that the minimum Mg-Si distance in Fig. 2(a) is1.311 Å, whereas it is0.958 Å, in Fig. 2(b).

This highly anisotropic distortion going to be the reason for improving the bond energy through reduction of distance between Sr-Si atoms in Sr-doped variant. We will discuss its effect on some properties of Sr doped Mg2Si in coming sections.

The k-point grid is used to discretize the integral necessary to obtain the total energy of the system. Hence, the mesh plays a key role in determining the level of convergence of the total energy value. The energy cut-off value is necessary to truncate the plain-wave expansion of the basis set for wave functions. Higher, the energy cut-off value, better the accuracy but more is the computational time. Hence, we see that the optimum values for these two parameters define the convergence of total energy for a system. In our calculation the optimized value for k-mesh is 6x6x6 and for energy cut-off value is 300 eV, shown in Figure 3 (a, b).

3.2 Electronic structure

The calculated electronic structures for Mg_2Si and 2x1x1MgSrSi supercell are shown in Fig. 4. From the electronic band structure, Fig. 4(a)), we can see that the valence band maxima (VBM) is located at Γ point and the conduction band minima is located at X point with an indirect band gap of 0.222 eV. It is observed that from partial dose shown in Fig. 4(a), the valence band mainly constructed from the Si atom. In the valence band at the Γ point, the energy is flat and degenerate. As you move from Γ point to X or L point, the energy become non-degenerate. For the case of Sr doped $Mg_{2-x}\,Sr_x$ Si of a 2x1x1supercell case when x = 1, Fig. 4(b), a narrow direct band gap at Γ point with a value of 0.195 eV separates the valence band, mostly comprising in large amount by Si orbitals, some contribution of Mg orbitals and very small contribution of Sr orbitals. It confirmed that Mg_2Si semiconductor shows metallic nature when it doped with Sr atom. The conduction band is highly dominated by Mg states; and smaller contributions from Sr- and Si-states with almost equal amounts. It indicates that the carrier concentration of Mg_2Si thermoelectric material increased when it doped with Sr-atom. After the doping, the fermi level shifts towards the conduction band. The most significant observation is that, even with a localized defect atom (Sr), the density of states projected to Sr states shows that the electrons from the dopant are spread over the entire crystal and are not localized in the region of the band gap. In the valence band at the Γ point, the energy looks like non-degenerate and flat. It is clearly observed in Fig. 4(b), that the energy is non-degenerate when moving from Γ-point to S- or Y-point.

3.3 Dynamic stability

Table 1 shows elastic properties of the calculated Mg_2Si and 2x1x1 Mg_2Si + Sr, in comparison with previous experimental data. The elastic stiffness tensor C_{ij} of a cubic crystal has three independent components, C_{11}, C_{12}, and C_{44}. Baraneck et al. [31, 32] reported the use of several ab initio methods to calculate the C_{ij} of Mg_2Si, using DFT (density functional theory) calculations to obtain more satisfactory results than HF calculations (Hartree-Fock-Roothaan).

Therefore, the agreement between the calculation and the experiment is satisfactory and its stability justified by Boron-Huang's lattice dynamic theory and satisfied the rule: $C_{11} > 0, C_{44} > 0, C_{11} - C_{12} > 0,\ C_{11} + 2C_{12} > 0$.

Our calculated results show good agreement with first principles calculation and experimental results, which verifies the stability of both systems. As values of elastic stiffness tensor (C_{11} , C_{12} & C_{44}) of the 2x1x1 Mg_2Si + Sr supercell is greater than the elastic stiffness tensor values of Mg_2Si shown in Table 1, Sr doped Mg_2Si is more stable than the undoped Mg_2Si. This conforms that Sr doped Mg_2Si has higher covalent character, i.e., higher bond energy than the pure Mg_2Si due to the distance between Sr-Si (0.968 Å) is less than the distance between Mg-Si (1.311 Å). See the discussion in section, 3.1.

3.4 Optical Properties

In Fig. 5(a), for the pure Mg_2Si, there is a strong hybridization between the Si-p, Mg-s and Mg-p orbitals, which indicate that the Mg and Si atoms form strong covalent bonds with each other. What is more, the Si-s has weak hybridization with Si-p, Mg-s and Mg-p orbitals.

In Fig. 5(b), for 2x1x1MgSrSi, there is a strong hybridization between the Sr-s, Si-p, Mg-s and Mg-p orbitals and indicates that the covalent bonds formed by Sr, Si, and Mg atoms is very strong. The presence of strong covalent bond between the constituent atoms conform that stability of the system which was justified by Boron-Huang's lattice dynamic theory, discussed in the previous section. The difference of the PDOS in Mg_2Si and 2x1x1MgSrSi is that the Sr-s and Sr-d orbitals in 2x1x1MgSrSi have strong hybridization.

The optical properties of a solid are usually described in terms of the complex dielectric function$\varepsilon = \varepsilon_1(\omega) + \varepsilon_2(\omega)$. The knowledge of the dielectric function allows the calculation of important optical functions. The calculated dielectric function for pure Mg_2Si and Sr-doped Mg_2Si is shown in Fig. 6. The threshold peak of ε_2 appearing at 2.4 eV for pure Mg_2Si and 2.2 eV for Sr-doped Mg_2Si is related to direct transitions along Γ directions. Above the main peak, the next peak centered at ~4.3 eV arises mainly from direct transitions at the L edge for Mg_2Si.

3.5 Electrical transport properties

Fig. 7 shows the Seebeck coefficient of pure and doped Mg2Si thermoelectric materials as a function of temperature. The Seebeck coefficient of pure Mg2Si semiconductor is greater than the

Sr-doped Mg2Si semiconductor material in all ranges of temperature. But in general, the Seebeck coefficient of Sr doped is increased with increasing temperature as a result of scattering of electrons with the vibration of lattices. As Sr is doped in Mg2Si the concentration of electrons in the system increases which leads to strong electron-phonon scattering and it became predominant over an increase in the electron concentration at higher temperatures. The Seebeck coefficient increases with the increment of carrier concentration and high carrier scattering. The Seebeck coefficient has a negative sign which shows that in the doped system the conduction is due to electrons. This also gives evidence that Sr is an n-type dopant in Mg2Si.

Fig. 8 shows electrical conductivity as a function of the temperature of doped and undoped Mg2Si thermoelectric materials. As the temperature of pure Mg2Si semiconductor material increases, its electrical conductivity also increases. But for the doped Mg2Si system, the mobility of charge carriers is very a result of the high concentration of the carriers. As a result the electrical conductivity slightly increases with increasing temperature. This is, increases in carrier concentration are compensated by a decrease in carrier mobility. The electrical conductivity of Sr doped has a higher value than the pure Mg2Si system due to the increase of carrier concentration. This justified that the Sr-doped Mg2Si thermoelectric material has lesser bandgap energy due to the introduction of impure energy level between the valance and conduction band but very close to the maximum valance band.

Fig 9 shows the electronic part of thermal conductivity as a function of temperature. The electronic thermal conductivity of undoped Mg2Si has a lesser value than Sr-doped Mg2Si material, due to Sr-s and Sr-d orbitals exhibiting strong hybridization bonds and contributing more charge carriers.

4. Conclusion

Pseudopotential method with GGA approximation has been used to study the thermoelectric properties of Sr doped Mg2Si material. Seebeck coefficient increases with increasing temperature, but Sr doped Mg2Si material has a lesser Seebeck coefficient than the pure Mg2Si system. Sr-doped Mg2Si materials exhibited enhanced electrical conductivity and electronic part of thermal conductivity increasing temperature, whereas pure Mg2Si material showed the same trend with temperature but with lesser values as compared with the doped one. Sr doped Mg2Si shows n-type conduction i.e., the conduction is due to electrons. The changes in electrical conductivity, Seebeck coefficient, and thermal conductivity are due to the increase in carrier concentration. Sr-doped

Mg2Si was found to be a better thermoelectric material with increased Seebeck coefficient, electrical conductivity, and corresponding electronic thermal conductivity at a high-temperature range.

Acknowledgements

The authors, thankful to the Jimma Institute of Technology for giving access to use computational laboratories.

Data availability statement: All data generated or analyzed during this study are included in this published article.

References

[1] Semiconducting Silicides, in: V.E. Borisenko (Ed.), Semiconducting Silicides, Springer, Berlin, 2000.

[2] D.M. Rowe, CRC Handbook of Thermoelectrics, CRC Press, Boca Raton, 1994 ch. 23–25.

[3] M.A. Khan, et al., In-situ heavily p-type doping of over 1020 cm−3 in semiconducting BaSi2 thin films for solar cells applications, Appl. Phys. Lett. 102 (2013) 112107.

[4] R.J. LaBotz, D.R. Mason, D.F. O'Kane, J. Electrochem. Soc. 110 (1963) 127.

[5] E.N. Nikitin, V.G. Bazanov, V.I. Tarasov, Sov. Phys. Solid State 3 (1962) 2648.

[6] Y. Noda, H. Kon, Y. Furukawa, N. Otsuka, I.A. Nishida, K. Masumoto, Mater. Trans. JIM 33 (1992) 845.

[7] J.Q. He, S.N. Girard, J.C. Zheng, L.D. Zhao, M.G. Kanatzidis, V.P. Dravid, Strong phonon scattering by layer structured PbSnS2 in PbTe based thermoelectric materials, Adv. Mater. 24 (32) (2012) 4440.

[8] W.S. Liu, B.P. Zhang, J.F. Li, L.D. Zhao, Effects of Sb compensation on microstructure, thermoelectric properties and point defect of CoSb3 compound, J. Phys. D Appl. Phys. 40 (21) (2007) 6784.

[9] J.Q. He, I.D. Blum, H.Q. Wang, S.N. Girard, J. Doak, L.D. Zhao, J.C. Zheng, G. Casillas, C. Wolverton, M. Jose-Yacaman, D.N. Seidman, M.G. Kanatzidis, V.P. Dravid, Morphology control of nanostructures: Na-doped PbTe-PbS system, Nano Lett. 12 (11) (2012) 5979.

[10] J.W. Zhang, L.R. Song, G.K.H. Madsen, K.F.F. Fischer, W.Q. Zhang, X. Shi, B.B. Iversen, Designing high-performance layered thermoelectric materials through orbital engineering, Nat. Commun. 7 (2016) 10892.

[11] G.D. Li, U. Aydemir, M. Wood, W.A. Goddard, P.C. Zhai, Q.J. Zhang, G.J. Snyder, Defect-controlled electronic structure and phase stability in thermoelectric skutterudite CoSb3, Chem. Mater. 29 (9) (2017) 3999.

[12] Jinfeng Yang, Jingyu Li, Chi Zhang, Zhenzhen Feng, Beibei Shi, Wenya Zhai, Yuli Yan, Yuanxu Wang, Excellent thermoelectric performance of BaMgSi driven by low lattice thermal conductivity: A promising thermoelectric material, Journal of Alloys and Compounds 827 (2020) 154342.

[13] V. K. Zaitsev et al., "Highly effective Mg2Si(Sn) thermoelectrics", Phys. Rev. B ,74, 045207 (2006)

[14] H.L. Liu, X. Shi, F.F. Xu, L.L. Zhang, W.Q. Zhang, L.D. Chen, Q. Li, C. Uher, T. Day, G.J. Snyder, Copper ion liquid-like thermoelectrics, Nat. Mater. 11 (5) (2012) 422.

[15] L.D. Zhao, S.H. Lo, Y.S. Zhang, H. Sun, G.J. Tan, C. Uher, C. Wolverton, V.P. Dravid, M.G. Kanatzidis, Ultralow thermal conductivity and high thermoelectric figure of merit in SnSe crystals, Nature 508 (7496) (2014) 373.

[16] X. Shi, J. Yang, J.R. Salvador, M.F. Chi, J.Y. Cho, H. Wang, S.Q. Bai, J.H. Yang, W.Q. Zhang, L.D. Chen, Multiple-filled skutterudites: high thermoelectric figure of merit through separately optimizing electrical and thermal transports, J. Am. Chem. Soc. 133 (20) (2011) 7837.

[17] S.I. Kim, K.H. Lee, H.A. Mun, H.S. Kim, S.W. Hwang, J.W. Roh, D.J. Yang, W.H. Shin, X.S. Li, Y.H. Lee, G.J. Snyder, S.W. Kim, Dense dislocation arrays embedded in grain boundaries for high-performance bulk thermoelectrics, Science 348 (6230) (2015) 109.

[18] Z.W. Chen, B.H. Ge, W. Li, S.Q. Lin, J.W. Shen, Y.J. Chang, R. Hanus, G.J. Snyder, Y.Z. Pei, Vacancy-induced dislocations within grains for high-performance PbSe thermoelectrics, Nat. Commun. 8 (2017) 13828.

[19] B. Poudel, Q. Hao, Y. Ma, Y.C. Lan, A. Minnich, B. Yu, X.A. Yan, D.Z. Wang, A. Muto, D. Vashaee, X.Y. Chen, J.M. Liu, M.S. Dresselhaus, G. Chen, Z.F. Ren, High-thermoelectric performance of nanostructured bismuth antimony telluride bulk alloys, Science 320 (5876) (2008) 634.

[20] Z.W. Chen, B.H. Ge, W. Li, S.Q. Lin, J.W. Shen, Y.J. Chang, R. Hanus, G.J. Snyder, Y.Z. Pei, Vacancy-induced dislocations within grains for high-performance PbSe thermoelectrics, Nat. Commun. 8 (2017) 13828.

[21] B. Poudel, Q. Hao, Y. Ma, Y.C. Lan, A. Minnich, B. Yu, X.A. Yan, D.Z. Wang, A. Muto, D. Vashaee, X.Y. Chen, J.M. Liu, M.S. Dresselhaus, G. Chen, Z.F. Ren, High-thermoelectric performance of nanostructured bismuth antimony telluride bulk alloys, Science 320 (5876) (2008) 634.

[22] Q.H. Zhang, Z.X. Zhou, M. Dylla, M.T. Agne, Y.Z. Pei, L.J.Wang, Y.S. Tang, J.C. Liao, J. Li, S.Q. Bai, W. Jiang, L.D. Chen, G.J. Snyder, Realizing high-performance thermoelectric power generation through grain boundary engineering of skutterudite-based nanocomposites, Nanomater. Energy 41 (2017) 501.

[23) Villars, P.; Cenzual, K. Pearson Crystal's Data-Crystal Structure Database for Inorganic Compound; ASM International: Materials Park, OH, USA, 2010/11.

[24] W. Li, S.Q. Lin, B.H. Ge, J. Yang, W.Q. Zhang, Y.Z. Pei, Low sound velocity contributing to the high thermoelectric performance of Ag8SnSe6, Adv. Sci. 3 (11) (2016) 1600196.

[25] W. Li, L.L. Zheng, B.H. Ge, S.Q. Lin, X.Y. Zhang, Z.W. Chen, Y.J. Chang, Y.Z. Pei, Promoting SnTe as an eco-friendly solution for p-PbTe thermoelectric via band convergence and interstitial defects, Adv. Mater. 29 (17) (2017) 1605887.

[26] L.W. Fu, M.J. Yin, D. Wu, W. Li, D. Feng, L. Huang, J.Q. He, large enhancement of thermoelectric properties in n-type PbTe via dual-site point defects, Energy Environ. Sci. 10 (9) (2017) 2030.

[27] H.J. Monkhorst, J.D. Pack, Special points for Brillouin-zone integrations, Phys. Rev. B 13 (1976) 5188-5192.

[28] Yu Z, Xie Q, Xiao Q and Zhao K, Acta Phys. Sin.58 (2009), 6889.

[29] Madsen, G. K. H.; Singh, D. J. BoltzTrap. A Code for Calculating Band-Structure Dependent Quantities. Comput. Phys. Commun. 2006, 175, 67−71.

[30] Mulualem Abebe, Kumar Brajesh, Anupam Mishra, Anatoliy Senyshyn, and Rajeev Ranjan, PHYSICAL REVIEW B 96, 014113 (2017).

[31] P. Baranek, J. Schamps, I. Noiret, J. Phys. Chem. B 101 (1997) 9147.

[32] P. Baranek, J. Schamps, J. Phys. Chem. B 103 (1999) 2601.

Figures

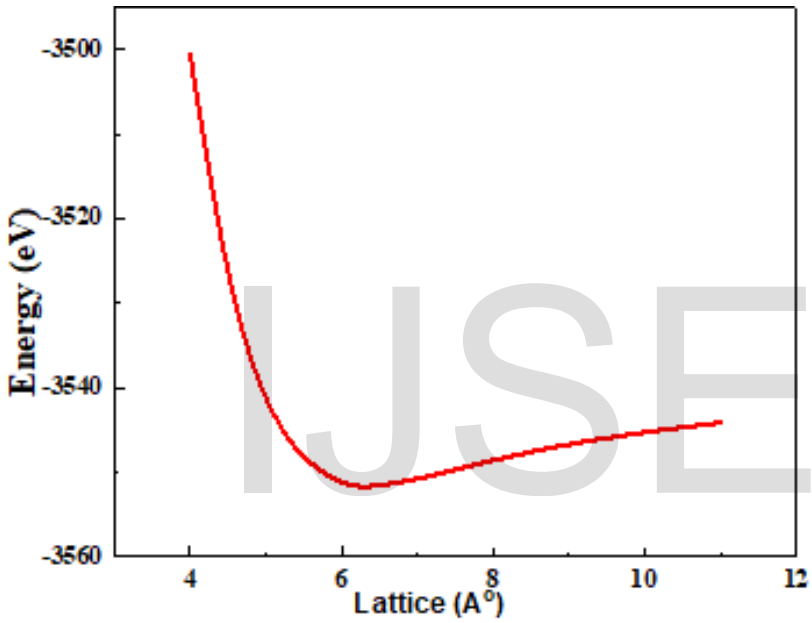

Figure 1 Calculated total energy versus unit cell lattice parameter of Mg_2Si for crystal structure of cubic Fm-3m phase.

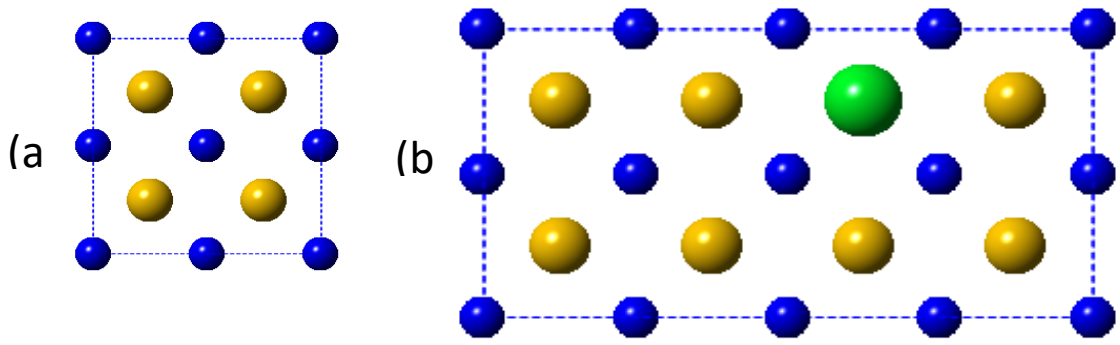

Figure 2 Crystal structure of (a) unit cell of Mg_2Si (b) 2x1x1 MgSrSi supercell with cubic Fm-3m phase.

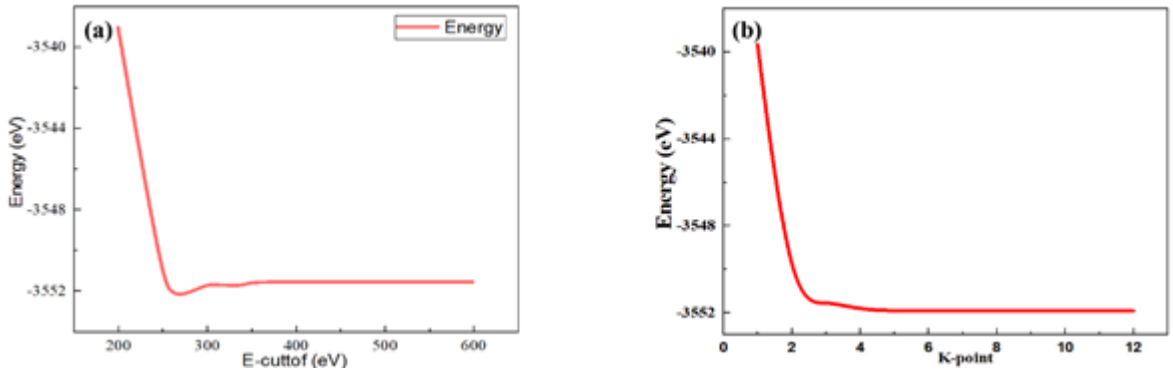

Figure 3 The optimum values for obtaining the converged results correspond to (a) a k-mesh of 6 x 6 x 6 and (b) ecutwfc of 300 eV.

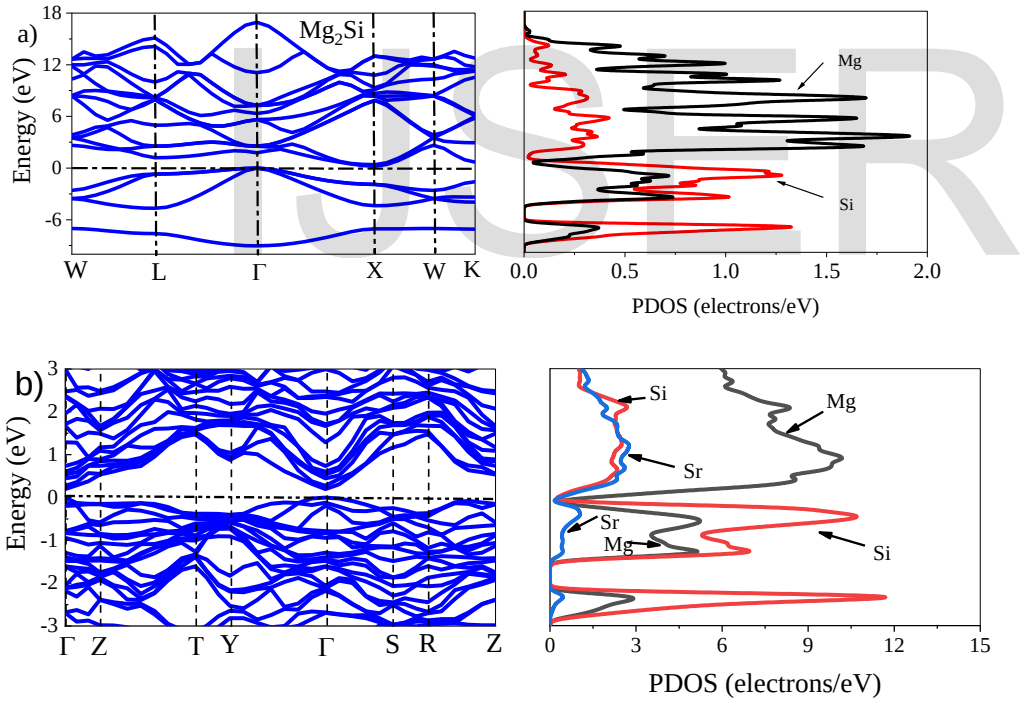

Figure 4 Band structures (left) and partial density of states plots (right) for (a) pure Mg2Si, (b) 2x1x1MgSrSi super cell.

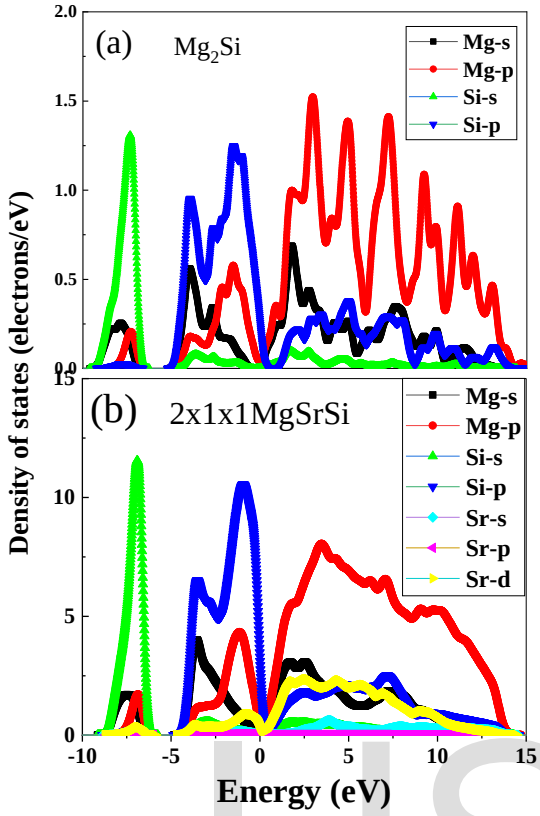

Figure 5 The partial dos state of (a) Mg2Si and (b) 2x1x1MgSrSi thermoelectric materials..

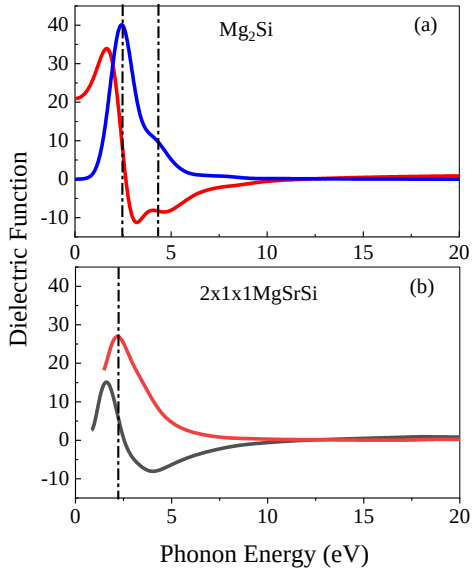

Figure 6 The dielectric function for (a) Mg2Si and (b) 2x1x1MgSrSi thermoelectric materials.

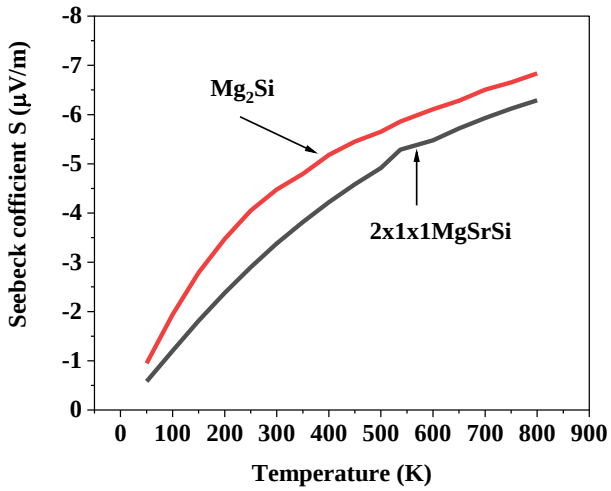

Figure 7 Variation of Seebeck Coefficient with temperature of Mg $_{2-x}$ Sr$_x$ Si material

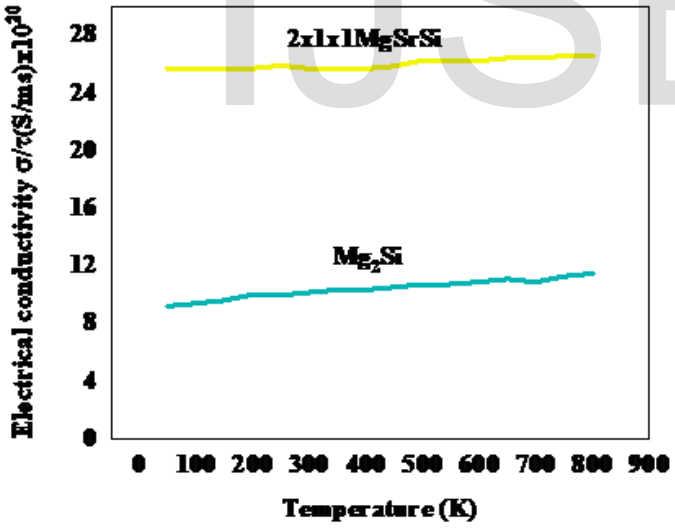

Figure 8 Variation of Electrical Conductivity with temperature of Mg $_{2-x}$ Sr$_x$ Si material

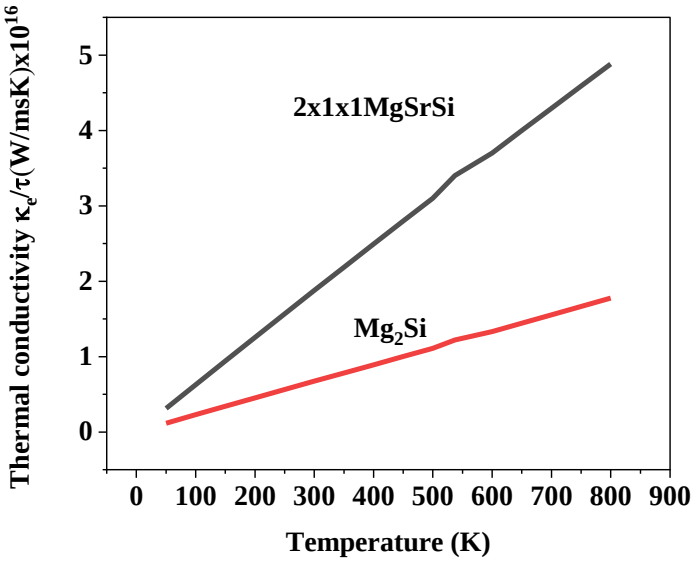

Figure 9 Variation of Electronic Thermal Conductivity with temperature of $Mg_{2-x}Sr_xSi$ material

Table 1 Elastic properties of the calculated Mg2Si and 2x1x1Mg_2Si supercell + Sr in comparison with previous experimental data.

compound	Properties	This Work (Calculated)	Experiment
Mg_2Si	Elastic Constant (GPa)		
	C_{11}	114.100	126[a]
	C_{12}	21.990	26[a]
	C_{44}	44.690	48.5[a]
	Elastic Constant (GPa)		
2x1x1Mg_2Si supercell + Sr	C_{11}	128	
	C_{12}	26.2	
	C_{44}	49.7	

[a]Ref. [31].